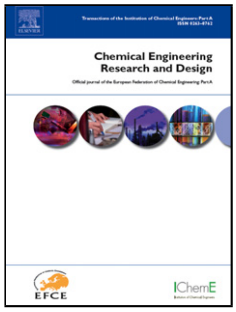

Title: Selective laser sintering of ceramic powders with bimodal particle size distribution

Authors: Daniele Sofia, Roberto Chirone, Paola Lettieri, Diego Barletta, Massimo Poletto

PII: S0263-8762(18)30293-4
DOI: https://doi.org/10.1016/j.cherd.2018.06.008
Reference: CHERD 3216

To appear in:

Received date: 26-3-2018
Revised date: 2-6-2018
Accepted date: 4-6-2018

Please cite this article as: Sofia, Daniele, Chirone, Roberto, Lettieri, Paola, Barletta, Diego, Poletto, Massimo, Selective laser sintering of ceramic powders with bimodal particle size distribution.Chemical Engineering Research and Design https://doi.org/10.1016/j.cherd.2018.06.008

Selective Laser Sintering of ceramic powders with bimodal particle size distribution

Daniele Sofia[a*], Roberto Chirone[b], Paola Lettieri[b], Diego Barletta[a], Massimo Poletto[a]

a. Dipartimento di Ingegneria Industriale, Università degli Studi di Salerno, Via Giovanni Paolo II, 132-I-84084 Fisciano (SA), Italy

b. Department of Chemical Engineering, University College London, London WC1E 7JE, UK

***Corresponding author. Tel. +39 089964014; Fax +39 089964057;E-mail address: dsofia@unisa.it**

Highlights

- Laser sintering applied on narrow sized and bimodal glass and ceramic powders
- Measured layer thickness, mass and mechanical strength of sintered specimen
- A model developed to describe the effect of composition in bimodal powders
- A key role is played by the connection force between coarse and fine particles
- Activating this connection force can significantly improve the material strength

Abstract

This paper addresses the possibility of carrying out Selective laser sintering (SLS) using powders obtained as mixtures of particles of different size. The beam source used in the experiments was a CO_2 laser tube with a nominal power of 40W. The materials used were model Glass beads and a real ceramic material characterized by irregular shape of the particles. Bimodal distributed powders were

generated by mixing samples characterized by different narrow particle size distributions. Single layer sintered specimens were obtained with a laser scanning speed of 50 mm/s and 8W beam. The sintered specimens were studied by means of microphotography and were characterized in terms of bulk density and tensile strength. Results show that the strength of the sintered specimen is significantly dependent upon the amount of fines in the powder mixture, in spite of the limited effects on the specimen thickness and density. In particular, the highest strength of the sintered material are observed with the highest fraction of fines in the originating powder mixture. In order to estimate the value of the forces between particles of different size produced by the sintering action, the model developed by Liu et al.,(2017), based on the Rumpf, (1958) approach, was purposely adapted. The application of the model revealed that in our process conditions the connection between large and fines particles is significantly weaker than the force between particles of the same size. The model also indicates that the strength of the sintered materials from mixtures can potentially increase up to values significantly higher than those of the materials sintered starting from the unimodal powder components.

Keywords: Laser sintering, powder distribution, Morphology analyses.

1. Introduction

Additive manufacturing technologies are changing the production processes in many sectors and include biomedical applications (Liu et al., 2007; Luo et al., 2014), metallurgical processes (Ojala et al., 2016), production of aerospace parts (Gu et al., 2012)etc. Among these technologies Selective Laser Sintering (SLS) and Selective Laser Melting (SLM) are two of the most promising processes ones. In these processes, a controlled laser beam is used to produce localized powder sintering or melting, according to the released power on the surface of a powder bed. Both techniques allows to

obtain three dimensional objects with an additive technique including a layer by layer powder bed formation (Chen et al., 2016).

Most of the current applications of SLS/SLM make use of metal or polymeric powders. With the most recent developments these technologies have been improved to create functional objects directly from metal powders without the use of either post-processing operations or of binders (low melting additives) (Greiner et al., 2017). Further application of these technologies can derive from the use of ceramic materials. One of the main issues related to the use of ceramic materials in SLS and SLM processes is the fragility of the manufactured objects, and the low density and poor surface finish of the sintered materials (Klocke and Ader, 2003). It has been proven that the high residual stresses in the internal structure of these objects is the major responsible for such fragility. These residual stresses are mainly due to high inhomogeneity of the internal temperature in the forming object during the process (Tang and Yen, 2004). Traditional sintering processes do not have these disadvantages (Kamyabi et al., 2017) but SLS and SLM might be preferred because the objects produced can be significantly more complex and much more easily customizable (Olmos et al., 2009).

In general in all sintering processes the strength of the artefact depends directly on the strength of the necks of the molten material that solidifies between the powder particles during the process (Ellis et al., 2014). The parameters that mostly affect the strength of the sintered materials are the process temperature, pressure and time. For example, it has been found that time and pressure are responsible for the strength of agglomerates of ash particles in conventional sintering (Fatt Teoh et al., 2012; Luan and You, 2015).

The discrimination between SLS and SLM is labile. In fact, it is mainly related to the amount of energy released to the material by the laser beam during the sintering/melting process (Franco and Romoli, 2012). SLS may have the advantage over SLM of producing smaller contraction of the processed material due to the less significant change of volume in the sintered particulate than in the melted one (Qian and Shen, 2013). Therefore, it is useful to understand how the initial material properties and the process conditions interact with each other to determine the degree of

sintering/melting of the raw material powder, as well as the mechanical properties of the sintered material.

With specific reference to SLS, most of the relevant investigations in the literature show that laser sintering is a very complicated process, with several parameters influencing the densification mechanism and affecting the final microstructural features of the produced objects (Liu et al., 2011). In general, research and applications with SLS make use of powders made of particles of the same kind. Nevertheless, with ceramics, new sintered materials with tailored characteristics might more easily produced by using powders obtained from the mixtures of particles characterized by different properties. The proper development of SLS using such mixtures would require an in depth knowledge of the contemporary sintering action of the laser on particles with different properties. In this paper, we propose an experimental procedure to understand the sintering action on powders made as mixtures of samples differing only by particle size. To this end, two different materials are used, namely a model material made of glass beads and a real powder made of ceramic particles with a highly irregular shape. A model based on the Rumpf approach will be proposed to calculate the strength of the necks between particles of different size.

2. Experimental methods

2.1 Apparatus

Figure 1 reports a sketch of the apparatus used for the experiments. A laser tube generates the laser beam which is collimated by a dedicated system to the exact target position. The CO_2 laser tube emits beams of maximum 40 W at a wavelength of 10.6 μm. The beam is collimated by a couple of 45° inclined mirrors moved on two orthogonal directions on the laser plane. The attained laser spot size is of 100 micron diameter. The collimating system allows to achieve a scan velocity of the laser spot on the illuminated plane in the range between 1 mm s^{-1} and 100 mm s^{-1}. The 40 W of the nominal

laser power allows to reach on the laser spot sufficiently high temperatures to produce the melting of ceramic particles up to hundreds of micrometers. The melting or sintering action of the laser beam on the powder hit by the laser beam on the illuminated plane can be controlled by adjusting the laser power and its speed. Alternative action of partial (selective) sintering of deposited layers and addition of new materials in new layer allows to obtain three dimensional objects, artefacts, characterized by complex geometries, immersed in a powder bed. In order to keep fixed the relative distance between the planar surface of the added layer and the laser source, before each layer addition, the powder bed is lowered down with a displacement equal to the thickness of the layer to be added. The construction of the 3 d object can be successful only if the thickness of each added powder layer is thin enough to be wholly penetrated by the sintering action of the laser beam. In this paper only experiments producing single layer artefacts will be considered.

In industrial SLS processes, powder layers are generally prepared thank to the spreading action of dedicated tools, such as blades or rollers. The quality of the surface of the powder generated depends on both the powder flowability and the operating parameters of the spreading tools. Powder flowability can be adjusted with the help of flow aids and regulated together with the operating parameters of the spreading tools in order to optimize the quality of the formed layer with powders characterized by different flow properties. For the sake of simplicity and in order to compare results obtained with different powders characterized by different flowability a non conventional bed preparation procedure was adopted in this paper in order to obtain bed surfaces of similar quality with different powders. In particular, a dedicated apparatus was used to contemporarily consolidate the powder bed and level its surface before the laser sintering action was applied. Figure 1 b) shows this apparatus, which consists in a flat lid connected to a cylindrical rod constrained by linear bearings to move vertically and to rotate around its axis. A loading plate on top of the rod is used to apply weights, whose load allows to adjust the desired powder compaction stress exerted by the lid. In order to ease the uniform powder compaction a twisting action of the lid is applied during the bed compaction, by rotating the rod with the help of a lever.

2.2 Preparation of materials

Two different materials were used in the experiments. The two material include Glass beads and ceramic powder. This latter was provided by an undisclosed industrial partner. As shown in example pictures of the materials reported in Figure 2, Glass beads, in soda-limestone glass, are characterized by a round regular shape, while the ceramic particles have a rather irregular shape provide with sharp edges. Both materials were sieved in order to obtain powder samples with narrow PSD. For each of the sieved samples, Table 1 reports the nominal ranges of the particle size of the original batches, the undersize and oversize sieve meshes used to produce each sample, the mean Sauter diameter, d_i, of the sample measured by means of a laser scattering measurement device (Malvern Mastersizer 2000), as well as the bulk density of the samples. The particle density was measured with a helium pycnometer and it is equal to 2500 kg m^{-3} for Glass and 2320 for the ceramic powder.

Binary mixtures were prepared by mixing in different proportions different couples of sieved samples. Proper mixing was accomplished by using a Turbula Mixer T2F. No measurement could be carried out to evaluate any mixing index to characterize the mixing state of the powder, which was only qualitatively evaluated by direct inspection. For an easy reference to the mixtures used in the sintering process, a code made of a letter and a number will be used. The letter will identify the 6 different couples of mixed sieved samples identified by the Sauter mean diameter: A, mixtures of 27 and 160μm Glass beads; B, mixtures of 86 and 184μm Glass beads; C, mixtures of 27 and 184μm Glass beads; D, mixtures of 48 and 184μm Glass beads; E, mixtures of 22.5 and 104.2 μm Ceramic material; F, mixtures of 51.0 and 104.2 μm Ceramic material. The number on the mixture code will identify the mass fraction of fines in the mixed sample: 0, 0% of fines; 1, 20% of fines; 2, 40% of fines; 3,

60% of fines; 4, 80% of fines; 5, 100% of fines. A summary of this classification criteria is reported in Table 2.

2.3 Procedures

Single layer specimens of sintered materials were obtained on the laser apparatus described above. A square geometry 10x10 mm was adopted for the specimens. Prior to each sintering test, 50 mm ID plastic caps were filled with the desired powder mixture in order to obtain cylindrical beds of powder samples. These were levelled and consolidated at 2.5 kPa and two 90° twists operated with the powder consolidation apparatus described above. The sintering of specimens was obtained by moving the laser on 51 parallel lines 10 mm long at a distance of 0.2 mm from each other. The laser power and the laser scanning speed were set to 8 W and 50 mm s^{-1}, respectively. This combination corresponds to a scanning energy of 160 J m^{-1}. This energy resulted to be sufficient to obtain sintered specimen with all the unimodal powders samples prepared with glass bead and with the ceramic material.

After the sintering process the sintered specimens were carefully collected, and their mass was measured with an analytical balance (300 Crystal).

To relate the sintering process parameters to the tensile strength of the sintered materials, the point flexural bending tests were carried out on the squared sintered specimens. From the results of the bending test it is possible to estimate the specimen thickness, its bulk density and the tensile strength of the sintered material. Details of the method are reported in the connected publication on methods (Sofia et al., 2018b).

3. Experimental results

A detailed report on the results of the sintering procedure applied to unmixed samples of glass beads, including all nominal particle sizes included in Table 1, is reported elsewhere (Sofia et al, 2018a). An

example of the microstructure of a sintered specimen of ceramic powders is given in Figure 3. As already observed for glass beads, the surface appearance is completely different on the two specimen sides, the one directly hit by the laser beam and the other one. In particular, a high degree of material melting is obtained on the former. The initial particle geometry is not visible anymore and the molten material collects in lumps whose size is not dependent on the initial particle size, but seems to be governed by the surface tension of the liquid (Shartsis and Smock, 1947). On the other side, only very limited effects of the sintering action is seen and the sintered particles show almost unchanged shapes. Figure 4 shows the specimen mass, the specimen thickness and the tensile strength of the sintered ceramic materials as a function of the particle size. It can be observed that the specimen mass increases slightly with the particle size while its thickness is almost constant, indicating an increase of the bulk density of the sintered material that follows the same trend of the original powder bulk density. The strength of the material shows instead a marked maximum for 22.5 μm particle size, indicating a different effectiveness of the dissipated laser power during the sintering process. A more detailed analysis of this phenomenon is available elsewhere Sofia et al., (2015). It was found that the energy required for the sintering process depends on the particle size. In particular, the amount of the energy supplied by the laser beam that is dispersed by different mechanisms of energy transfer changes with the particle size. The energy dispersion fluxes were estimated on the base of experiments to evaluate the process effectiveness in particle melting or sintering. Tensile strength of unimodal samples for both materials are summarized in Table 1. Inspection of the table and Figure 4 reveals that for Glass beads the maximum strength is attained for the specimen with a nominal particle size of 48 μm. Ceramic particle provide a maximum at 22 μm in Table 1.

Figure 5 reports the results of the sintering procedure applied on glass mixtures A, all made with particles of 27 (fine) and 160 μm (coarse) mean Sauter diameter. Figure 5 is organized in the form of a table. In the Figure, each line reports the images of the specimen obtained from a mixture with a

different content of the fine component. The first line reports the results obtained sintering a powder entirely made with the coarsest fraction (160 μm), or 0% of fines, and it is indicated with the label 0, according to Table 2. The last line of Figure 5 shows images of the sintered specimens obtained sintering a powder entirely made with the finest fraction (27 μm), or 100% of fines, and it is indicated with the label 5, according to Table 2. In column M of the Figure, macro photographs of the whole 10x10 mm specimens are reported, while in columns F, R and T optical microscopy pictures (about 100x) of the front, back and lateral views of sintered specimens are reported.

Inspection of Figure 5 indicates that moving towards higher fines contents modifies the process from sintering into melting. In fact, single particles are visible on both specimen sides up to 60% fines content and up to 80% considering the backside only. In all the cases reported it appears that the residual particles on the front side are smaller than the particles on the backside, suggesting some particle coalescence phenomena on the more energized side. A layer of well adhering particles is visible on the backside of all the specimens, independently of the fines content in the initial powder samples.

Lateral views do not show significant differences in the thickness of the specimen, suggesting that the fines content does not affect the absolute penetration ability of the laser beam. Further indications on the effectiveness of laser penetration can be obtained by the data of specimen masses and of layer thicknesses reported in Figure 6a and 6b. Both the specimen mass and thickness slightly decrease with the content of fines, a part from the thickness at 100% content of fines. Figure 6c reports results of the tensile strength of the sintered specimen measured with the bending test and relevant to the specimen back size. Data point and error bars in the figure are the results of 5 independent experiments. Inspection of the figure indicates that the tensile strength of the material increases steadily with the fines content. In particular, it appears that all mixtures (20-80% of fines) provide results which are intermediate between those of the single components. Similar measures, with

qualitatively similar results were carried out with all the mixtures included in Table 2. The complete set of results is reported in the connected publication on methods (Sofia et al., 2018b). Figure 6 reports, as a further example, the results obtained with mixture E of the ceramic material.

4. Discussion

The macroscopic properties of sintered artifacts will depend upon their microscopic structure, that is the spatial density and the strength of the sintered contacts (necks). It might be argued that, in case of particle sintering (i.e. in case of limited melting of the particles in the original powder system) the spatial organization of particles can be assumed similar to the initial spatial organization of the particles in the powders prepared for the laser sintering process. For powders, a simple approach that allows to relate mechanical properties of powders with the strength of the contact forces between particles is the Rumpf (1958) approach modified according to Molerus (1975) suggestion, which allows to estimate both the interparticle contact density and their role in the definition of powder strength. This approach has used several times in the past in studies related to powder agglomeration (i.e Boerefijn et al., 2008; Pietsch, 1991; Russell et al., 2015; Schubert, 1975) or in the study of powder tensile strength (i.e. Castellanos et al., 2007; Valverde et al., 1998), as well as the study of powder flow properties at ambient conditions (Liu et al., 2017; Tomas, 2007), at high temperature (i.e. Chirone et al., 2018, 2016; Liu et al., 2018; Macrì et al., 2017b, 2017a; Tomasetta et al., 2011) and in humid air (Landi et al., 2011).

In the following, the Rumpf (1958) approach modified according to Molerus (1975) suggestion will be used to relate the strength of the sintered material with the strength of single necks in it.

In the Rumpf and Molerus, model some simplifying assumptions are made, in particular it is assumed that:

1. particles are organized in a randomly packed assembly and particles are spherical and monodisperse;

2. the contact areas between particles are small enough in comparison with the particle surface and, therefore, contact areas can be assumed as contact points;
3. the contact points are distributed over the particle spherical surface with equal probability;
4. the packing structure is isotropic;
5. The transmission of an isostatic state of stress with three equal principal stresses is assumed and therefore all the inter-particle forces are normal to the particle surface.

Starting from these hypotheses, Rumpf (1970) and Molerus (1975) derived the following equation relating the isostatic stress, σ_{iso}, with a mean isotropic contact force, F:

$$\sigma_{iso} = F \frac{k\phi}{\pi d_p^2} \tag{1}$$

where d_p is the particle diameter, ϕ the space volume fraction of the particles and k the particle coordination number. The double footer on the symbol F_{ii} is to recall that in this general case it is assumed that the interparticle contact force is the one between particles of same size. According to the correlation derived by Rumpf, (1958) from the experimental data of Smith et al. (1929) obtained for spherical particles and values of the particle concentration between 0.55 and 0.65, the empirical relationship $k(1-\phi) \approx \pi$ is assumed to estimate k:

$$k = \frac{\pi}{(1-\phi)} \tag{2}$$

This simple model will be used to calculate the strength of the necks in the sintered material of the specimen obtained from unimodal powder samples. These neck strengths will be used in a similar model approach, modified in order to account for bimodal particle distribution in powder samples and to predict the strength of the derived sintered specimens. The detail of this procedure is given in the following.

Using experiments on sintered materials with unimodal narrow PSD it is possible to use equations (2) and (3) to estimate the contact force of the sintered contact, F_{ii}, for each average particle diameter,

$d_{i,}$ starting from experimental values of the breakage modulus σ_{bi} of the sintered material made exclusively from particles of the same diameter d_i:

$$F_{ii} = \sigma_{bi} \frac{\pi d_i^2}{3.1\phi_i}(1-\phi_i) \tag{3}$$

For unimodal samples, the specific particle space volume fraction ϕ_i can be related to the experimental powder bulk density, ρ_{bi}, and the particle density, ρ_p:

$$\phi_i = \frac{\rho_{bi}}{\rho_p} \tag{4}$$

The results of this calculation are provided in Table 1 for both materials. As it is possible to observe from this table, expectedly the particle coordination number k_i is increasing with the system bulk density, but in any case it is much smaller than the theoretical value of 12, proper of the maximum packing density of equally sized spheres. The force of the sintered contact F_{ii} increases with the particle diameter, suggesting larger sintering necks for larger particles. Assuming as a reference for the material tensile strength σ_{tm} a value of 100 MPa for glass (Cai et al., 2016) and of 600 MPa for the ceramic material (Chirone et al., 2016) it is possible to use the values of F_{ii} to estimate the contact neck size, d_{ci}:

$$d_{ci} = \sqrt{\frac{4F_{ii}}{\sigma_{tm}\pi}} \tag{5}$$

As expected, the contact neck size increases with the particle diameter and, in any case, appears to be fully compatible with the particle diameters. One of the basic assumptions behind the model adopted in the Rumpf (1958) approach modified according to Molerus (1975) is that the particles are spherical. The ceramic particles, instead, are rather angular. However, provided that the particle shape is isometric (*i.e.* it does not show any prevailing size in one or two directions) the random position of the particles in the space can average any local particle preferential contact direction located on the sharper edges. Furthermore, as it appears from equation (3) it is the particle size that has the major

role in determining the relationship between interparticle forces and the strength of the agglomerate. Instead the role of the particle shape in determining the number of contact point (equation 3) might be only a second order effect, for coordination numbers around 6.

In order to find a quantitative relationship relating the microscopic forces between particles and the strength of the sintered specimens the Rumpf (1958) approach was modified in order to account for the bimodal particle size distribution. This model is a simplified version of a more general approach accounting for systems provided with a large particle size distribution and used by Liu et al. (2017) to relate the flow properties of real powders to the experimental properties of several narrowly sieved cuts. The main assumptions of this approach are coherent with assumption 1-5 of the Rumpf (1958) approach reported above, the only difference is that the assumption of monodisperse particles in point 1 is removed. Differently from the original model developed by Liu et al. (2017) for wide particle size distributions, in this case the bimodal powder is considered to be a model mixture of only two ideal monosized samples of powder. The particle size of these two ideal samples is set to the Sauter mean diameter of the two real cuts used for the real mixure.

Accordingly, it is assumed that the binary mixture is the result of 2 particle size components of the same material, each characterized by a single particle size, d_f and d_c for the fine and coarse cuts, respectively. Of course if r_f and r_c are the corresponding particle radii it is $d_f = 2r_f$ and $d_c = 2r_c$. In order to ease the calculation we will refer to the number fraction of each of the 2 component, v_f and v_c, which can be easily calculated from the component mass fraction, $f_f = f$ and $f_c = 1\text{-}f$ according to the following:

$$v_j = \frac{f_j / d_j^3}{\sum_{i=f,c}^{n} f_i / d_i^3} \qquad j = f, c \tag{6}$$

where j can be either f or c according to the component considered. Similarly, we will need to refer to the fraction, s_j, of the particle surface developed by each of the size component of the particles that can be calculated as follows:

$$s_j = \frac{f_j / d_j}{\sum_{i=f,c} f_i / d_i} \qquad j = f, c \tag{7}$$

Making particular the results obtained by Liu et al. (2017) it is possible to find the expression for the isostatic tensile strength of the material:

$$\sigma_{\mathrm{b},iso} = \frac{\phi_f + \phi_c}{\pi} \sum_{j=f,c} \nu_j d_j \sum_{i=f,c}^{n} k_{ji} F_{ji} \Bigg/ \sum_{j=f,c} \nu_j d_j^3 \tag{8}$$

Where k_{ji} the average number of contacts of particles of radius r_i on those of radius r_j, F_{ji} is the corresponding binary interaction force, ϕ_f and ϕ_f are the space volume fractions of the coarse and fine particles. Of course, i and j are equal in case we are considering particles belonging to the same component. It is worth noting that while $k_{fc} \neq k_{cf}$ we have that $F_{fc} = F_{cf}$. The details of the derivation of equation (8) obtained by applying the reasoning by Liu et al. (2017) to a binary mixture are reported in the Appendix.

In the case of mono-disperse particles systems, equation (9) will reduce to the original equation proposed by Rumpf (1958). However, for binary systems, the coordination numbers k_{ji} as well as the inter-particle forces F_{ji} should be sought for the application of equation (9).

According to Suzuki et al., (2008), k_{ji}, that is the average number of contacts between the particles of diameter d_i and those of diameter d_j, is:

$$k_{ji} = k\, s_i \left(2 - \sqrt{3}\right)\left(\frac{d_j}{d_i} + 1\right) \Bigg/ \left\{2\left[1 + \frac{d_j}{d_i} - \sqrt{\frac{d_j}{d_i}\left(\frac{d_j}{d_i} + 2\right)}\right]\right\} \qquad j, i = f, c \tag{9}$$

The parameter k is the coordination number of mono-sized spherical particles given by equation (3). It is assumed that the binary interaction forces between particles of the same size (F_{ff} and F_{cc}) are equal to the forces found for the sintered specimens of unimodal samples reported in Table 1. Then the set of equations (6) to (9) allows to predict the strength of sintered specimen, provided that the binary connection force between fine and coarse particles F_{fc} is defined, and assuming that there is

no difference between the isostatic tensile strength $\sigma_{b,iso}$ and the uniaxial tensile strength σ_b. In principle the force F_{fc} may depend on both the fine and coarse particle diameter as well as to the sintering process parameters, such as the laser power and to the particle exposure time to the laser. In the lack of direct information, this force should be considered as an adjustable parameter in our experiments and we have assumed that it is independent of the fines content in the mixture. Furthermore, this assumption is coherent with the other assumptions made that F_{ff} and F_{cc} are not affected by the fines content. Experimental and predicted values of the sintered material tensile strength for all bimodal mixtures used in the sintering process are reported in Figure 7 for glass and Figure 8 for the ceramic powder. Data point and error bars are the results of 5 independent experiments. The figure reports as dotted lines all model data obtained with the value of F_{fc} that minimizes the sum of the mean squared errors, in which the square errors between the model and each experimental point is weighed by the inverse of the experimental standard deviation of the point. The minimizing forces are reported in Table 2 for each of the binary systems at the different fines contents. It should be noted that in all the cases the values of F_{fc} are at least one order of magnitude lower than both the values F_{ff} and F_{cc} and that model results are only very slightly sensitive to changes of F_{fc} to different values of the same order or lower. In fact, the model results are almost coincident with those of the extremely limiting case in which F_{fc} is put to 0, as also shown in Figures 7 and 8 by model curves represented by hyphenated lines. Therefore, with the sintering process conditions relative to results reported in Figures 7 and 8. it can be concluded that the contribution to the strength of the bimodal sintered material due to the connection between particles of different diameter is not playing any role.

The whole set of model results obtained with the applications of eqs (7) to (11) with values of F_{fc} that minimizes the error with the experiment are given in the additional material.

A parametric study on the effect of the intensity of the connection force between particles of different size F_{fc} is reported in Figure 9. In particular, the specimen strength have been calculated for four different values of F_{fc} and namely F_{fc}=0, F_{fc}= F_{cc}/2, F_{fc}= F_{cc} and F_{fc}= F_{ff}. It appears clearly that it would be sufficient to activate the connection force between particles of different size to a value of the order the connection force between coarse particles to have a strength of mixture that is higher than those of the samples of the single components. The maximum of the strength increases significantly for higher values of F_{fc}. It can be concluded that the use of powder mixture including particles of different size might be adopted to significantly increase the strength of the sintered materials if it might be possible to use a procedure able to better activate the connection between particles of different size than we were able to do in our experiments.

In the hypothesis that it could be possible to activate the contact between coarse and fines in order to obtain F_{fc}= F_{cc}, Figures 8 and 9 report model calculations as continuous lines. It appears clearly that the maximum possible increase of the strength of the sintered material depends on the relative dimensions of the fine and coarse particles in the originating mixture. In order to highlight the effect of the ratio between the fine and coarse particle size in the strength of the artefact of a mixture, the maximum value of the difference between the model results for the artefact strength obtained with F_{fc}= F_{cc} and the experimental data, $\Delta\sigma_{max}$, has been found for the different mixtures tested. Figure 11, reports the ratio between $\Delta\sigma_{max}$ and the tensile strength obtained sintering coarse particles only, σ_{bc}, as a function of the fine to coarse particle diameter ratio d_f/d_c. It appears clearly that the increase of the strength of the material starts to be significant for fines particle size smaller that about 1/3 of the coarse particle size. It is also noteworthy that in this diagram the relative increments of the sintered material strength $\Delta\sigma_{max}/\sigma_{bc}$ are very similar for the two particle material tested.

5. Conclusions

Microscopic observations on sintered materials and measures of mass, thickness and strength of single layer artifacts allow to characterize the effect of the main parameters in the laser sintering process.

The observation of the artifacts at the microscope allows to verify that the granular material directly subjected to irradiation of the laser has a high degree of fusion, while on the opposite side to the scanned one, the particles retain the original geometry.

The mixing of powders of different sizes produces significant changes on the mechanical properties of the sintered material in spite of limited changes of the artifact produced in terms of thickness and density. In particular, the highest strength of the sintered material are observed with the highest fraction of fines in the originating powder mixture.

The model by Liu et al. (2017), which extended the relationship found by Rumpf (1958) between material strength and interparticle forces to systems provided with a particle size distribution, was used to understand the effectiveness of the sintering process on bimodal mixtures. In particular the application of the model revealed that in our process conditions the connection between large and fines particles is significantly weaker than the force between particles of the same size. Data available in the present research do not allow to understand the reason for that and it is only possible some speculative thinking. A possibility is that in large particles surrounded by small ones the amount of laser energy effectively used to heat up the large particles is dispersed with other mechanisms such as fast conduction to the fines. The model also indicates that the strength of the sintered materials from mixtures can increase up to values significantly higher than those of the sintered materials from the unimodal powder components, if it might be possible to use a procedure able to better activate the connection between particles of different size. In this case, the increase of strength would depend on the size ratio between fines and coarse and would requires fines that are smaller than about 1/3 of the coarse particles. The optimum fines content would be around 0.4 in mass fraction.

List of symbols

A area of the cutting plane in the Rumpf analysis, m^2

d_c Sauter mean diameter of the coarse particle fraction, m

d_f Sauter mean diameter of the fine particle fraction, m

d particle Sauter mean diameter, m

F contact strength, N

f_c mass fraction of the coarse particles, -

f_f mass fraction of the fine particles, -

F_{ij} contact strength between particles of size d_i and d_j, N

k particle coordination number, -

k_{ji} average number of contacts of particles of size d_j on those of size d_i, -

N_p number of particles per unit volume in the mixture, -

r_c Sauter mean radius of the coarse particle fraction, m

r_f Sauter mean radius of the fine particle fraction, m

S surface of the spherical cap of the particle cut by the reference palne in the Rumpf analysis, m^2

s_c mass fraction of the coarse particles, -

s_f mass fraction of the fine particles, -

Greek symbols

$\Delta\sigma_{max}$ maximum value of the difference between the model results for the artefact strength obtained with $F_{fc}= F_{cc}$, Pa

φ angle from the vertical of the cutting plane in the Rumpf analysis, -

ϕ space volume fraction of particles

ϕ_c space volume fraction of the coarse particles, -

ϕ_f space volume fraction of the fine particles, -

ϕ_i space volume fraction of particles of dimeter d_i, -

v_c number fraction of the coarse particles, -

v_f number fraction of the fine particles, -

ρ_{bi} bulk density of the sintered specimen of particles of diameter d_i, Pa

ρ_p particle density, Pa

σ_{bi} strength of the sintered specimen of particles of dimeter d_i, Pa

σ_b strength of the sintered specimen, Pa

σ_b strength of the sintered specimen, Pa

$\sigma_{b,iso}$ isostatic strength of the sintered specimen, Pa

σ_{iso} isostatic strength, Pa

σ_{tm} material tensile strength, Pa

ζ Distance from the cutting plane in the Rumpf analysis, m

References

Boerefijn, R., Dontula, P.-R., Kohlus, R., 2008. Detergent Granulation, in: Salman, A.D., Hounslow, M.J., Seville, J.P.K. (Eds.), Granulation.

Cai, D., Zhou, G., Silberschmidt, V. V., 2016. Effect of through-thickness compression on in-plane tensile strength of glass/epoxy composites: Experimental study. Polym. Test. 49, 1–7. https://doi.org/10.1016/j.polymertesting.2015.10.015

Castellanos, A., Quintanilla, M.A.S., Valverde, J.M., Quintanilla, M.A.S., Soria-Hoyo, C., 2007. Novel instrument to characterize dry granular materials at low consolidations. Rev. Sci. Instrum. 78, 73901. https://doi.org/10.1063/1.2751096

Chen, R.K., Jin, Y. an, Wensman, J., Shih, A., 2016. Additive manufacturing of custom orthoses and prostheses-A review. Addit. Manuf. 12, 77–89. https://doi.org/10.1016/j.addma.2016.04.002

Chirone, R., Barletta, D., Lettieri, P., Poletto, M., 2016. Bulk flow properties of sieved samples of a ceramic powder at ambient and high temperature. Powder Technol. 288, 379–387. https://doi.org/10.1016/j.powtec.2015.11.040

Chirone, R., Barletta, D., Poletto, M., Lettieri, P., 2018. Detection and estimation of capillary interparticle forces in the material of a fluidized bed reactor at high temperature by powder flow characterization. Powder Technol. 330, 371–385. https://doi.org/10.1016/j.powtec.2018.02.024

Ellis, A., Noble, C.J., Hopkinson, N., 2014. High Speed Sintering: Assessing the influence of print density on microstructure and mechanical properties of nylon parts. Addit. Manuf. 1, 48–51. https://doi.org/10.1016/j.addma.2014.07.003

Fatt Teoh, H., Tao, Y., Soon Tok, E., Wei Ho, G., Haur Sow, C., 2012. Direct laser-enabled graphene oxide–Reduced graphene oxide layered structures with micropatterning. J. Appl. Phys. 112, 064309. https://doi.org/10.1063/1.4752752

Franco, A., Romoli, L., 2012. Characterization of laser energy consumption in sintering of polymer based powders. J. Mater. Process. Technol. 212, 917–926. https://doi.org/10.1016/j.jmatprotec.2011.12.003

Greiner, S., Wudy, K., Lanzl, L., Drummer, D., 2017. Selective laser sintering of polymer blends: Bulk properties and process behavior. Polym. Test. 64, 136–144. https://doi.org/10.1016/j.polymertesting.2017.09.039

Gu, D.D., Meiners, W., Wissenbach, K., Poprawe, R., 2012. Laser additive manufacturing of metallic components: materials, processes and mechanisms. Int. Mater. Rev. 57, 133–164. https://doi.org/10.1179/1743280411Y.0000000014

Kamyabi, M., Sotudeh-Gharebagh, R., Zarghami, R., Saleh, K., 2017. Principles of viscous sintering in amorphous powders: A critical review. Chem. Eng. Res. Des. 125, 328–347. https://doi.org/10.1016/j.cherd.2017.06.009

Klocke, F., Ader, C., 2003. Direct laser sintering of ceramics. Solid Free. Fabr. Symp. 447–455.

Landi, G., Barletta, D., Poletto, M., 2011. Modelling and experiments on the effect of air humidity on the flow properties of glass powders. Powder Technol. 207, 437–443. https://doi.org/10.1016/j.powtec.2010.11.033

Liu, B., Wildman, R., Tuck, C., Ashcroft, I., Hague, R., 2011. Investigation the effect of particle size distribution on processing parameters optimisation in selective laser melting process, in: 22nd Annual International Solid Freeform Fabrication Symposium. University of Texas, Austin, pp. 227–238.

Liu, C., Xia, Z., Czernuszka, J.T., 2007. Design and development of three-dimensional scaffolds for

tissue engineering. Chem. Eng. Res. Des. 85, 1051–1064. https://doi.org/10.1205/cherd06196

Liu, Y., Lu, H., Barletta, D., Poletto, M., Guo, X., Gong, X., Jin, Y., 2018. Bulk flow properties of fly ashes at ambient and high temperature. Particuology 38, 113–125. https://doi.org/10.1016/j.partic.2017.04.013

Liu, Y., Lu, H., Poletto, M., Guo, X., Gong, X., 2017. Bulk flow properties of pulverized coal systems and the relationship between inter-particle forces and particle contacts. Powder Technol. 322, 226–240. https://doi.org/10.1016/j.powtec.2017.07.057

Luan, C., You, C., 2015. A novel experimental investigation into sintered neck tensile strength of ash at high temperatures. Powder Technol. 269, 379–384. https://doi.org/10.1016/j.powtec.2014.09.031

Luo, X., Liu, Y., Gu, C., Li, Z., 2014. Study on the progress of solidification, deformation and densification during semi-solid powder rolling. Powder Technol. 261, 161–169. https://doi.org/10.1016/j.powtec.2014.04.001

Macrì, D., Barletta, D., Lettieri, P., Poletto, M., 2017a. Experimental and theoretical analysis of TiO 2 powders flow properties at ambient and high temperatures. Chem. Eng. Sci. 167, 172–190. https://doi.org/10.1016/j.ces.2017.03.057

Macrì, D., Poletto, M., Barletta, D., Sutcliffe, S., Lettieri, P., 2017b. Analysis of industrial reactive powders flow properties at high temperature. Powder Technol. 316, 131–138. https://doi.org/10.1016/j.powtec.2016.10.064

Molerus, O., 1975. Theory of yield of cohesive powders. Powder Technol. 12, 259–275. https://doi.org/10.1016/0032-5910(75)85025-X

Ojala, L.S., Uusi-Kyyny, P., Alopaeus, V., 2016. Prototyping a calorimeter mixing cell with direct metal laser sintering. Chem. Eng. Res. Des. 108, 146–151. https://doi.org/10.1016/j.cherd.2015.11.015

Olmos, L., Martin, C.L., Bouvard, D., 2009. Sintering of mixtures of powders : Experiments and modelling. Powder Technol. 190, 134–140. https://doi.org/10.1016/j.powtec.2008.04.057

Pietsch, W., 1991. Size enlargement by agglomeration.

Qian, B., Shen, Z., 2013. Journal of Asian Ceramic Societies Laser sintering of ceramics. Integr. Med. Res. 1, 315–321. https://doi.org/10.1016/j.jascer.2013.08.004

Rumpf, H., 1958. Grundlagen und Methoden des Granulierens. Chemie Ing. Tech. - CIT 30, 144–158. https://doi.org/10.1002/cite.330300307

Russell, A., Schmelzer, J., Müller, P., Krüger, M., Tomas, J., 2015. Mechanical properties and failure probability of compact agglomerates. Powder Technol. 286, 546–556. https://doi.org/10.1016/j.powtec.2015.08.045

Schubert, H., 1975. Tensile strength of agglomerates. Powder Technol. 11, 107–119. https://doi.org/10.1016/0032-5910(75)80036-2

Shartsis, L., Smock, A.W., 1947. Surface Tensions of Some Optical Glasses. J. Am. Ceram. Soc. 30, 130–136. https://doi.org/10.1111/j.1151-2916.1947.tb18881.x

Smith, W. O., Foote, P. D., Busang, P.F., 1929. Packing of homogeneous spheres. Phys. Rev. 34, 1271–1274.

Sofia, D., Barletta, D., Massimo, P., 2018a. Laser sintering process of ceramic powders: the effect of particle size on the mechanical properties of sintered layers. Addit. Manuf. submitted.

Sofia, D., Chirone, R., Lettieri, P., Barletta, D., Poletto, M., 2018b. Methods of preparation of materials for the Selective Laser Sintering of ceramic powders with bimodal particle size distribution. MethodsX Submitted.

Sofia, D., Granese, M., Barletta, D., Poletto, M., 2015. "Laser Sintering of Unimodal Distributed Glass Powders of Different Size." Procedia Eng. 102, 749–758. https://doi.org/10.1016/j.proeng.2015.01.180

Suzuki, M., Shinmura, T., Iimura, K., Hirota, M., 2008. Study of the wall effect on particle packing structure using X-ray micro computed tomography. Adv. Powder Technol. 19, 183–195. https://doi.org/10.1163/156855208X293817

Tang, H.-H., Yen, H.-C., 2004. Ceramic Parts Fabricated by Ceramic Laser Fusion. Mater. Trans. 45, 2744–2751. https://doi.org/10.2320/matertrans.45.2744

Tomas, J., 2007. Adhesion of ultrafine particles-A micromechanical approach. Chem. Eng. Sci. https://doi.org/10.1016/j.ces.2006.12.055

Tomasetta, I., Barletta, D., Poletto, M., 2011. The Effect of Temperature on Flow Properties of Fine Powders, in: Chemical Engineering Transactions. pp. 655–660. https://doi.org/10.3303/CET1124110

Valverde, J.M., Ramos, A., Castellanos, A., Keith Watson, P., 1998. The tensile strength of cohesive powders and its relationship to consolidation, free volume and cohesivity. Powder Technol. 97, 237–245. https://doi.org/10.1016/S0032-5910(98)00025-4

Appendix

This appendix describes the derivation of equation (9) for the tensile strength of a artefact sintered starting from a bimodal mixture. Following the Rumpf (1958)approach described by Molerus (1975) and reported in Figure A1, the binary component mixture can be ideally cut by a plane. Therefore, the sintered specimen strength, considered as the limiting stress acting on the cut plane, can be calculated from the sum of all the forces that each particle transfers to the cutting plane from its surface in contact with other particles. The strength can be calculated as the sum of forces divided by the surface of the cutting plane. The force contribution of the particles belonging to each of the 2 components can be calculated separately and, then, summed up. Given a unit surface, it is important to define the number of the particles of each of the 2 component cut by the plane. If N_p is the number of particles per unit volume in the mixture, the number of particles of radius r_j is $N_p v_j$ and, since the volume per unit surface that is occupied by the particles of radius r_j that are cut by the plane is $2r_j$, the number of particles of this component cut by the plane is $2N_p v_j r_j$. If, in turn, we take only the particles of radius r_j that have their center at a distance between ζ and $\zeta + d\zeta$ from the plane, then the number is $2N_p v_j r_j \cdot d\zeta / r_j = 2N_p v_j d\zeta$. The contribution of the sintered connections of these particles to

the strength on the cutting plane will be given by the sum of all the binary inter-particle connection strength acting on the spherical cap defined by cutting plane. The forces on this spherical cap depend on the binary interaction between the particle of radius r_j and the particles of both the fine and coarse component of the mixture. We call k_{ji} the average number of contacts between the particles of radius r_i and those of radius r_j. In particular, i and j may coincide in case we are considering particles belonging to the same component, namely k_{ff} and k_{cc}, and of course $k_{fc} \neq k_{cf}$. Furthermore, we call F_{ji} the binary interaction force that, according to the Rumpf (1958) hypotheses, is independent of the contact position. In this case the mutual action in a binary contact implies that $F_{fc} = F_{cf}$. Following the Molerus (1975) reasoning, we have that the contribution of the forces exerted on the cutting plane by a single particle cut of radius r_j with the center at a distance between ζ and $\zeta + d\zeta$ is:

$$\int_{S(\zeta)} \sum_{i=f,c} \frac{k_{ji}}{4\pi r_j^2} F_{ji} \cos\varphi dS = \frac{1}{4\pi r_j^2} \sum_{i=f,c} k_{ji} F_{ji} \int_{S(\zeta)} \cos\varphi dS = \frac{1}{4\pi r_j^2} \sum_{i=f,c} k_{ji} F_{ji} \pi\left(r_j^2 - \zeta^2\right) \quad j = f,c \tag{A1}$$

Where: $S(\zeta)$ is the surface of the spherical cap defined by the spherical particle cut by the plane at a distance ζ from the center; $F_{ji}\cos\varphi$ is the contact force component normal to the cutting plane; $k_{ji}/4\pi r_j^2$ is the probability per unit surface of the particle of radius r_j to be in contact with a particle of radius r_i; dS is the particle surface element, which is defined by a certain distance from the cutting plane, as depicted in Figure A1; $A_t(j, \zeta) = \pi (r_j^2 - \zeta^2)$ is the projected area on the cutting plane of the spherical cap of a particle of radius r_j cut at a distance ζ from the center. The isotropic properties of the powder make both k_{ij} and F_{ij} independent of the contact position and, therefore, in Eq. (A1) can be taken out of the surface integral. The force contribution of all the particles of radius r_j cut by the plane is:

$$\int_{-r_j}^{r_j} \frac{2N_p \nu_j}{4\pi r_j^2} \sum_{i=f,c} k_{ji} F_{ji} \pi\left(r_j^2 - \zeta^2\right) d\zeta = \frac{N_p \nu_j}{2r_j^2} \sum_{i=f,c} k_{ji} F_{ji} \int_{-r_j}^{r_j} \left(r_j^2 - \zeta^2\right) d\zeta = \frac{2}{3} N_p f_j r_j \sum_{i=f,c} k_{ji} F_{ji} \quad j = f,c \tag{A2}$$

The total force, F_t, on the cutting plane is given by the sum of the contribution due to both the 2 components of fine and coarse fractions:

$$F_t = \frac{2}{3} N_p \sum_{j=f,c} \nu_j r_j \sum_{i=f,c} k_{ji} F_{ji} \tag{A3}$$

In order to have the strength, this force has to be divided by the area, *A*, occupied by the particles cut by the ideal plane

$$A = \frac{1}{\phi_f + \phi_c} \sum_{i=f,c} \int_{-r_j}^{r_j} 2N_p \nu_j \int_{S(\zeta)} \cos\varphi dS = \frac{2N_p}{\phi_f + \phi_c} \sum_{i=f,c} \nu_j \int_{-r_j}^{r_j} \pi\left(r_j^2 - \zeta^2\right) d\zeta = \frac{8\pi}{3\left(\phi_f + \phi_c\right)} N_p \sum_{i=f,c} \nu_j r_j^3 \tag{A4}$$

The strength can be readily calculated as:

$$\sigma_{\mathrm{b},iso} = \frac{F_t}{A} = \frac{\phi_f + \phi_c}{4\pi} \sum_{j=f,c} \nu_j r_j \sum_{i=f,c} k_{ji} F_{ji} \Bigg/ \sum_{j=f,c} \nu_j r_j^3 = \frac{\phi_f + \phi_c}{\pi} \sum_{j=f,c} \nu_j d_j \sum_{i=f,c}^{n} k_{ji} F_{ji} \Bigg/ \sum_{j=f,c} \nu_j d_j^3 \tag{A5}$$

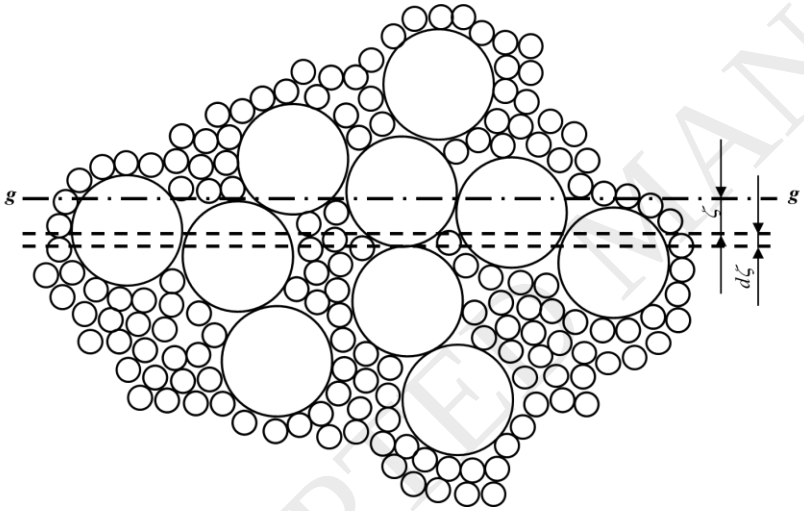

Figure A1. Schematic of the spatial configuration of bimodal powders. The visualized distance ζ, applies to the calculations for coarse particles (*j*=c) in fact it should be $\zeta < rj$.

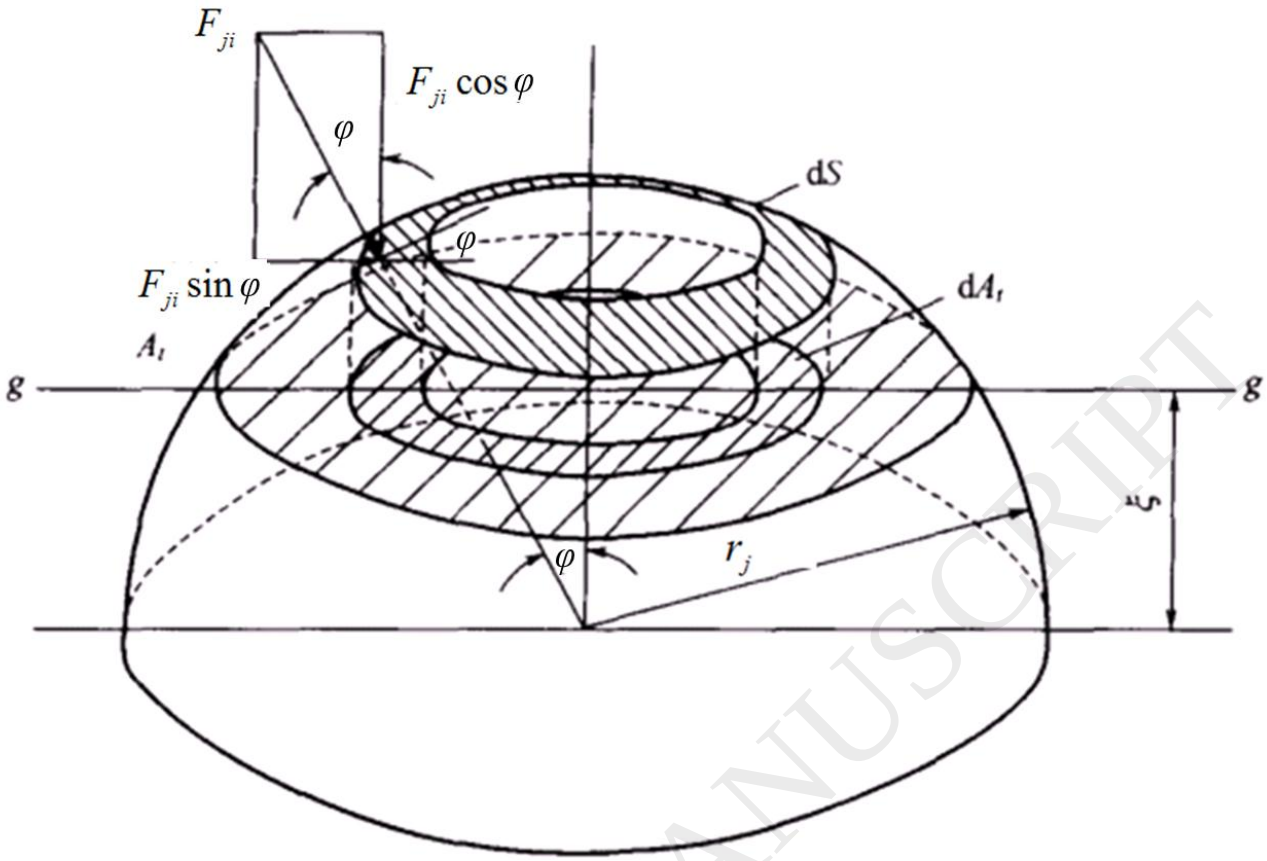

Figure . A2. Schematic of force analysis for a signal particle *j*. Adapted from Molerus (1975).

Table captions

Table 1. Properties of sieved powder samples.

Table 2. The coding scheme used for bimodal mixtures. The last line of the table reports the fine to coarse particle connection force F_{fc} found with a regression procedure of the model equation (8) on the experimental data relative to each couple of materials at all fines concentrations.

Figure captions

Figure 1. Experimental set-up. a) Apparatus of laser sintering: 1. laser tube; 2. scanning mirrors moving in x and y directions; 3. laser beam; b). Apparatus to consolidate and level beds of powders before the sintering process.

Figure 2. Micro images of typical sieved samples of materials. a) transmittance microphotography of 104 µm glass beads and b) SEM image of 125 µm ceramic material.

Figure 3. SEM microphotographs of sintered specimens obtained from 51 µm unimodal ceramic powders: a) front side; b) back side.

Figure 4. Properties of the 10x10 mm sintered specimens as a function of the nominal size of the initial unimodal powder sample of the ceramic material: a) thickness; b) mass; c) tensile strength on the specimen backside.

Figure 5. Macro and micro photographs of 10x10 mm sintered specimens obtained from bimodal powder mixtures A, by using a 8 W laser beam and a 50 mm s^{-1} laser scanning speed. Fines contents: 0, 0%; 1, 20%; 2, 40%; 3, 60%; 4, 80%; 5, 100%. M macroscopic view; F, front view; R back view; T, lateral view.

Figure 6. Properties of the 10x10 mm sintered specimens as a function of the fines content of the initial bimodal powder: a) thickness; b) mass; c) tensile strength on the backside. Connecting lines for: - -, Glass powder mixture A; —, Ceramic powder mixture E. :Data point and error bars are the results of 5 independent experiments.

Figure 7. Tensile strength of glass beads artefacts as a function of the fines contents for different powder mixtures used in the sintering process: a) MixA, 27 µm - 160 µm; b) MixB, 86 µm - 184 µm; c) MixC, 27 µm - 184 µm; d) MixD, 48 µm - 184 µm. Squares are experiments; error bars are standard deviations; lines are model results calculated with different values of the connection force between fine and coarse particles: ––, $F_{fc} = F_{cc}$; .- -, $F_{fc} = 0$; ⋯, F_{fc} minimizes the error with the experiments (values in Table 2). Data point and error bars are the results of 5 independent experiments.

Figure 8. Tensile strength of Ceramic material artefacts as a function of the fines contents for different powder mixtures used in the sintering process: a) MixE, 22.5 µm – 104.2 µm; b) MixF, 51 µm – 104.2 µm; c). Squares are experiments; error bars are standard deviations; lines are model results calculated with different values of the connection force between fine and coarse particles: ––, $F_{fc} = F_{cc}$; .- -, $F_{fc} = 0$; ⋯⋯, F_{fc} minimizes the error with the experiments (values in Table 2). Data point and error bars are the results of 5 independent experiments.

Figure 9. Model results of the sintered material strength as a function of the fines fraction calculated with different values of the connection force between fine and coarse particles: ⋯⋯, F_{fc}=0; ––, $F_{fc}= F_{cc}/2$, – · –$F_{fc}= F_{cc}$ and – –, $F_{fc}= F_{ff}$.

Figure 10. The maximum value of the difference ($\Delta\sigma_{max}$) between the model results for the artefact strength obtained with $F_{fc}= F_{cc}$ and the experimental data, referred to the tensile strength obtained sintering coarse particles only (σ_{bc}) plotted as a function of the fine to coarse particle size ratio d_f/d_c: •, Glass beads; ▲, Ceramic particles; - -, fitted line to guide the eye.

Figure A1. Schematic of the spatial configuration of bimodal powders. The visualized distance ζ, applies to the calculations for coarse particles (j=c) in fact it should be $\zeta < rj$.

Figure . A2. Schematic of force analysis for a signal particle j. Adapted from Molerus (1975).

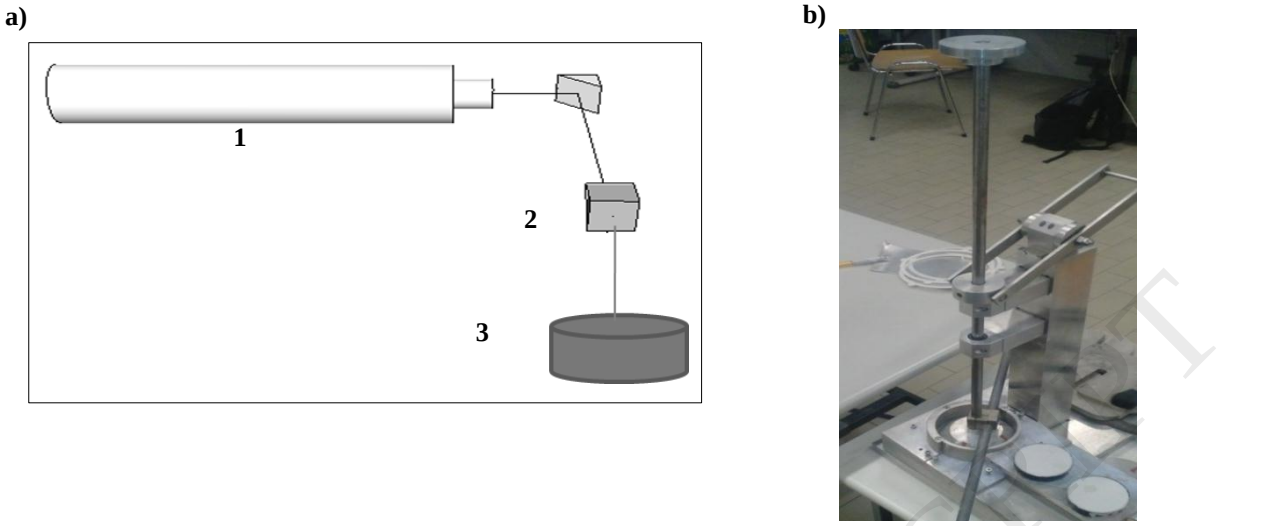

Figure 1. Experimental set-up. a) Apparatus of laser sintering: 1. laser tube; 2. scanning mirrors moving in x and y directions; 3. laser beam; b). Apparatus to consolidate and level beds of powders before the sintering process.

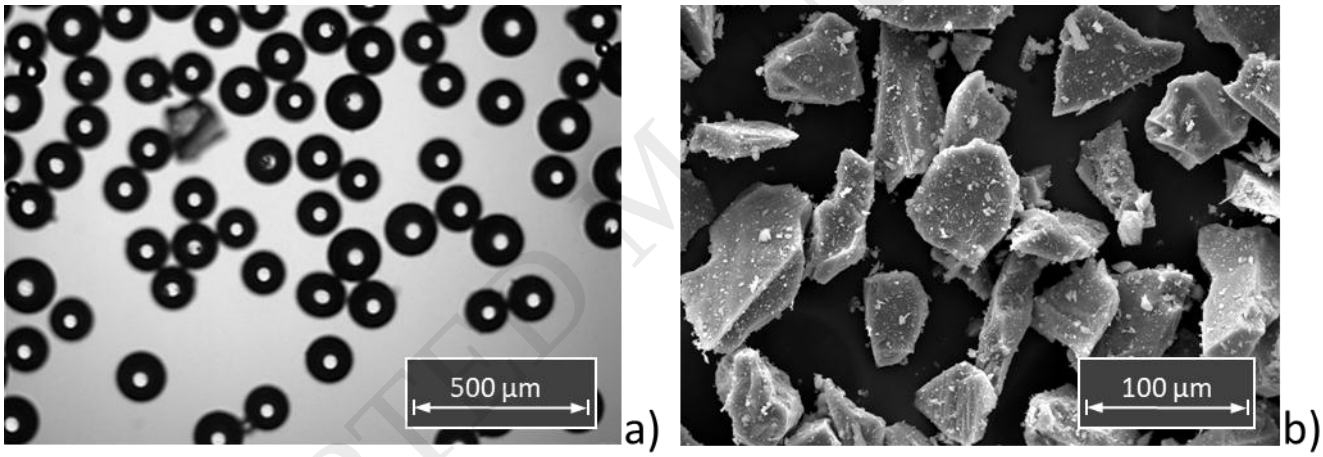

Figure 2. Micro images of typical sieved samples of materials. a) transmittance microphotography of 104 µm glass beads and b) SEM image of 125 µm ceramic material.

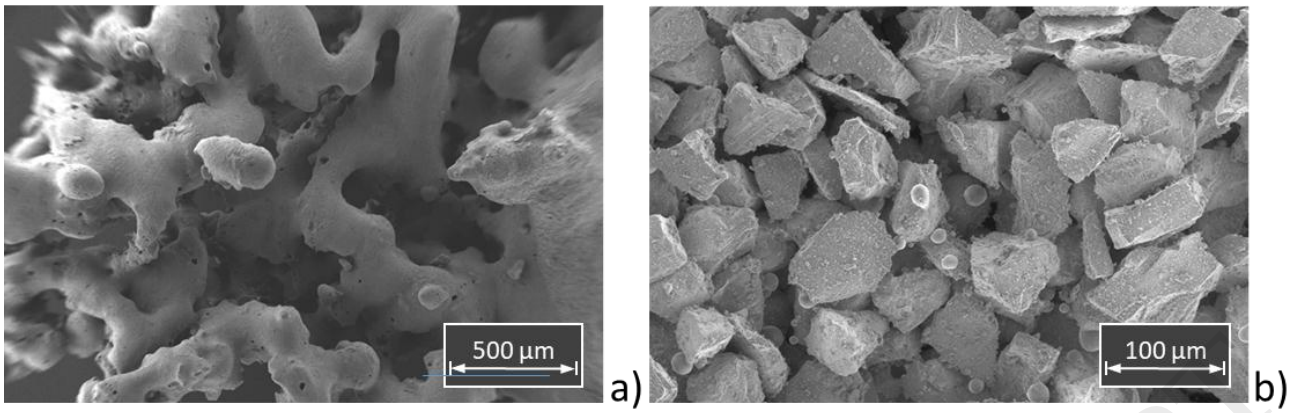

Figure 3. SEM microphotographs of sintered specimens obtained from 51 µm unimodal ceramic powders: a) front side; b) back side.

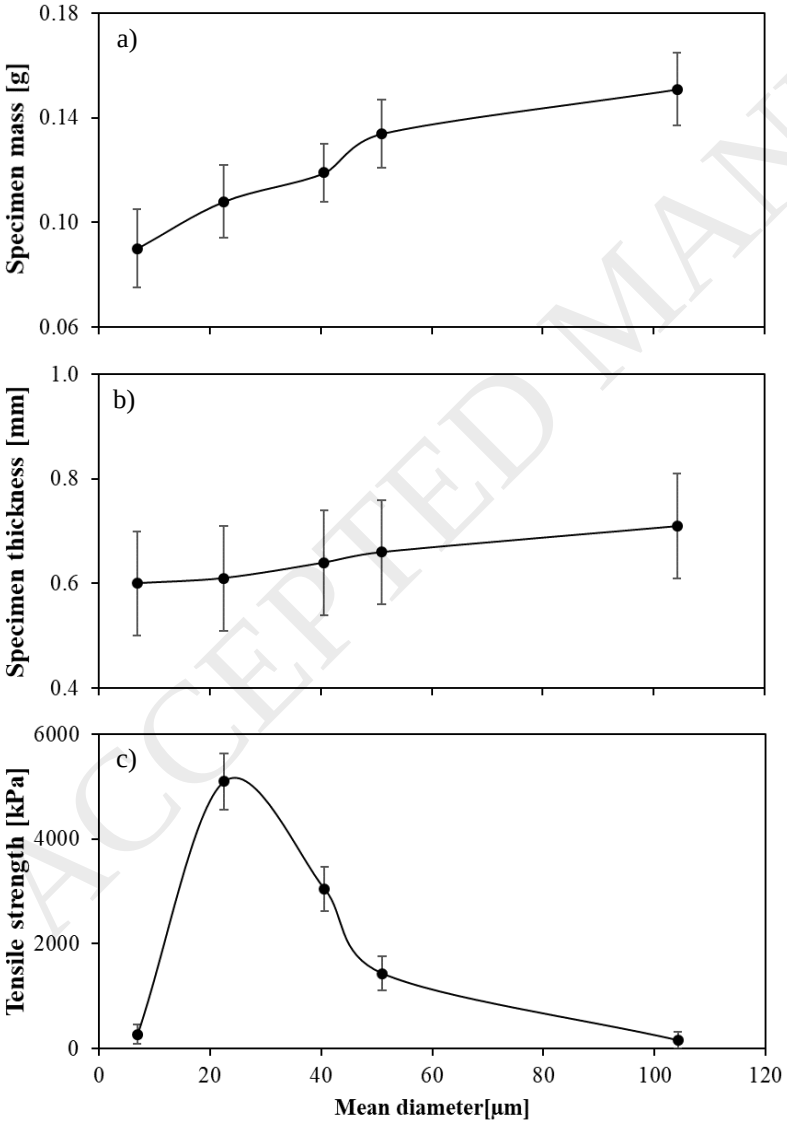

Figure 4. Properties of the 10x10 mm sintered specimens as a function of the nominal size of the initial unimodal powder sample of the ceramic material: a) thickness; b) mass; c) tensile strength on the specimen backside.

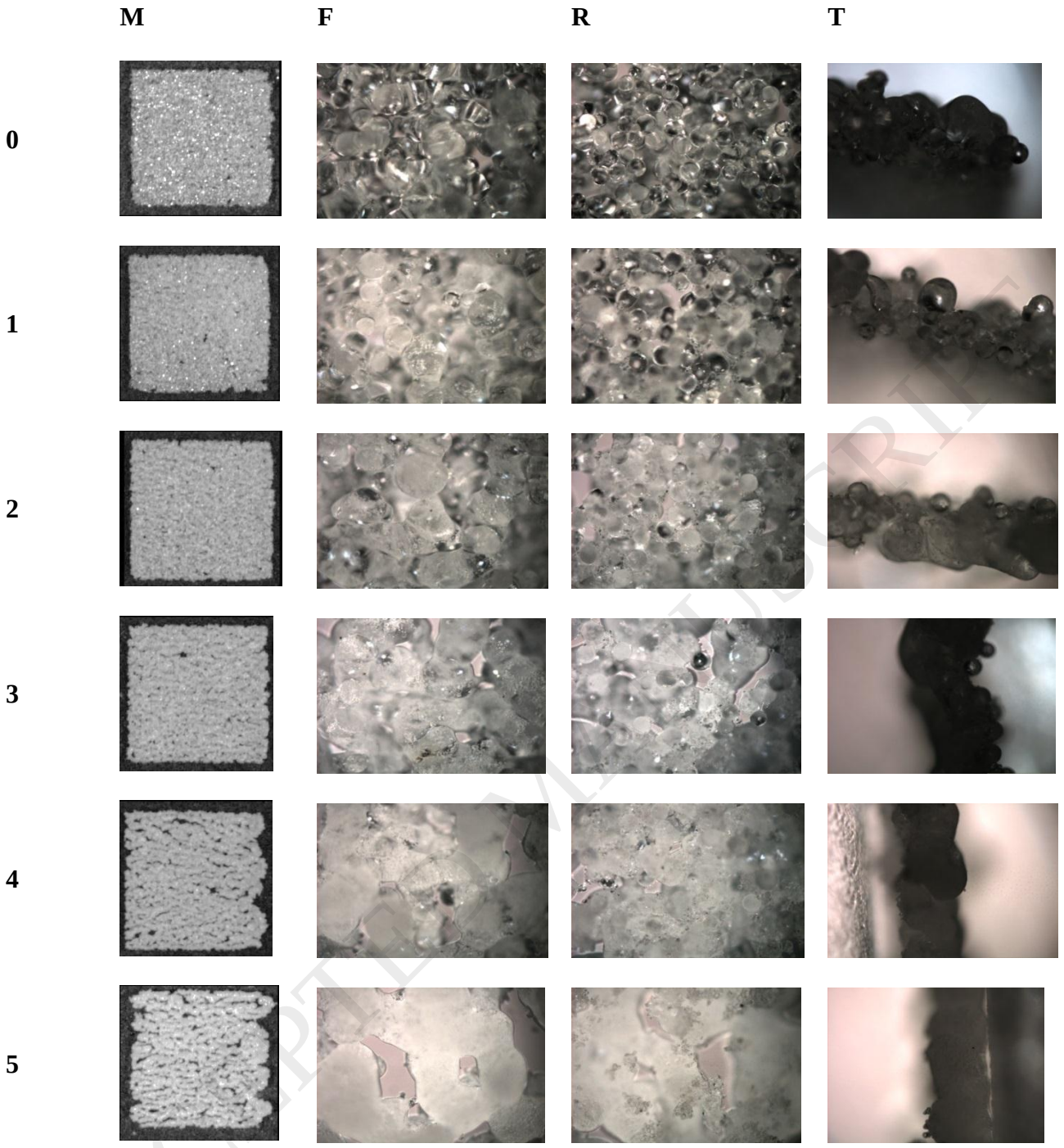

Figure 5. Macro and micro photographs of 10x10 mm sintered specimens obtained from bimodal powder mixtures A, by using a 8 W laser beam and a 50 mm s^{-1} laser scanning speed. Fines contents: 0, 0%; 1, 20%; 2, 40%; 3, 60%; 4, 80%; 5, 100%. M macroscopic view; F, front view; R back view; T, lateral view.

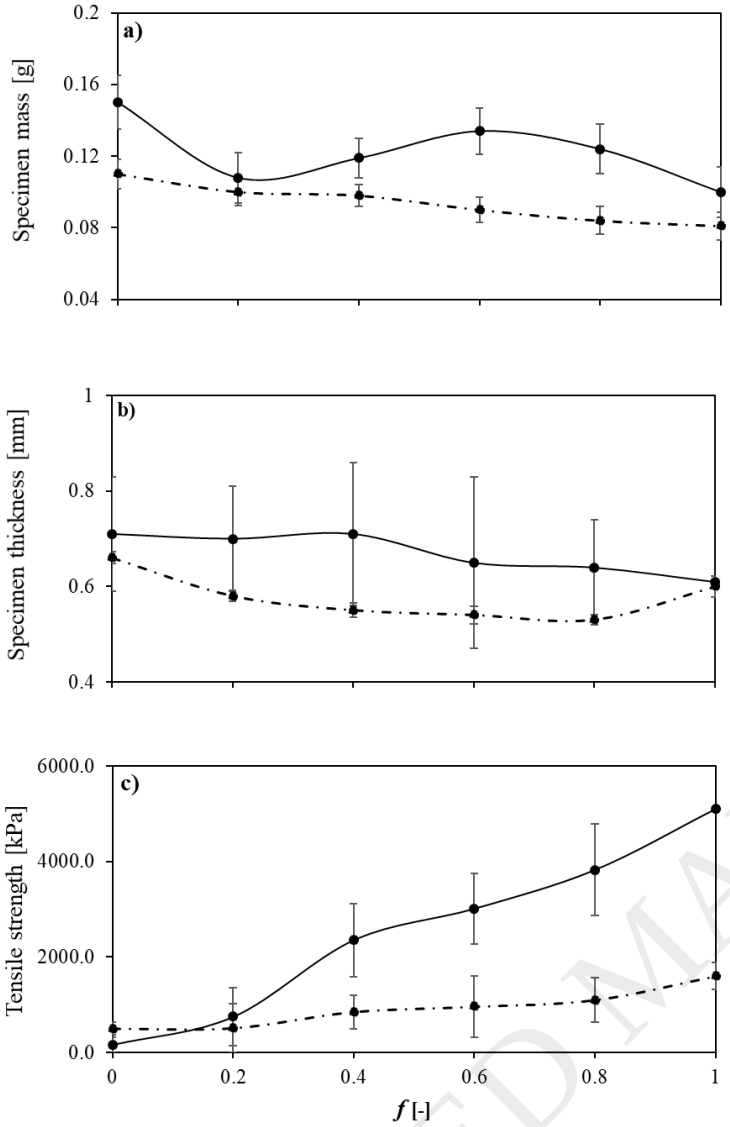

Figure 6. Properties of the 10x10 mm sintered specimens as a function of the fines content of the initial bimodal powder a) thickness; b) mass; c) tensile strength on the backside. Connecting lines for: - -, Glass powder mixture A; —, Ceramic powder mixture E. :Data point and error bars are the results of 5 independent experiments.

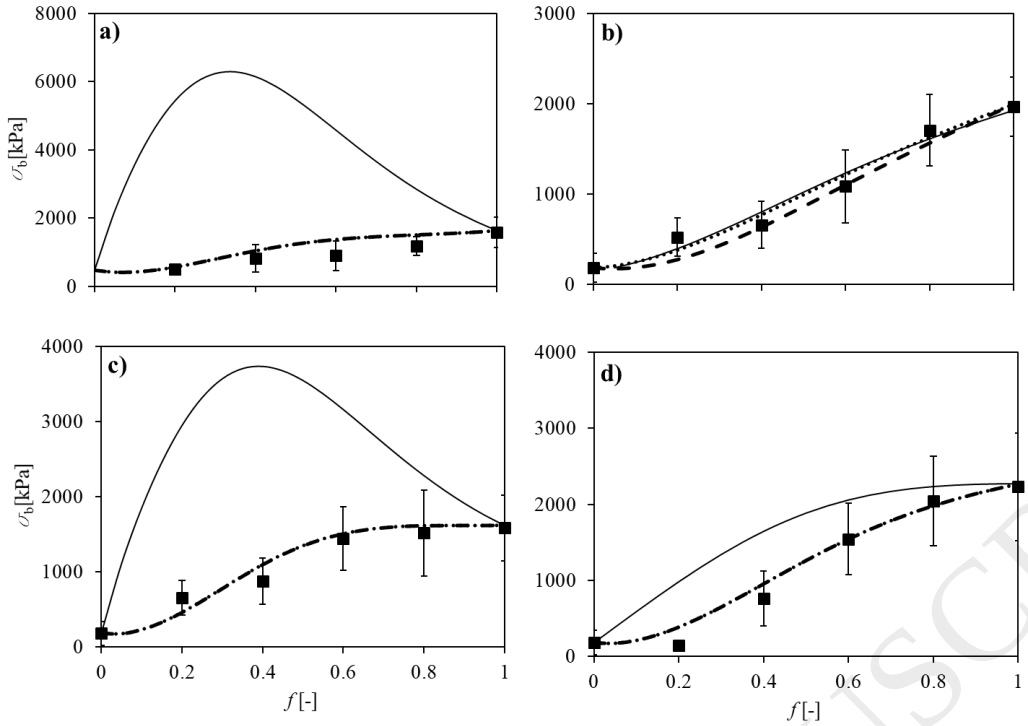

Figure 7. Tensile strength of glass beads artefacts as a function of the fines contents for different powder mixtures used in the sintering process: a) MixA, 27 µm - 160 µm; b) MixB, 86 µm - 184 µm; c) MixC, 27 µm - 184 µm; d) MixD, 48 µm - 184 µm. Squares are experiments; error bars are standard deviations; lines are model results calculated with different values of the connection force between fine and coarse particles: ––, $F_{fc} = F_{cc}$; .- -, $F_{fc} = 0$; ⋯, F_{fc} minimizes the error with the experiments (values in Table 2). Data point and error bars are the results of 5 independent experiments.

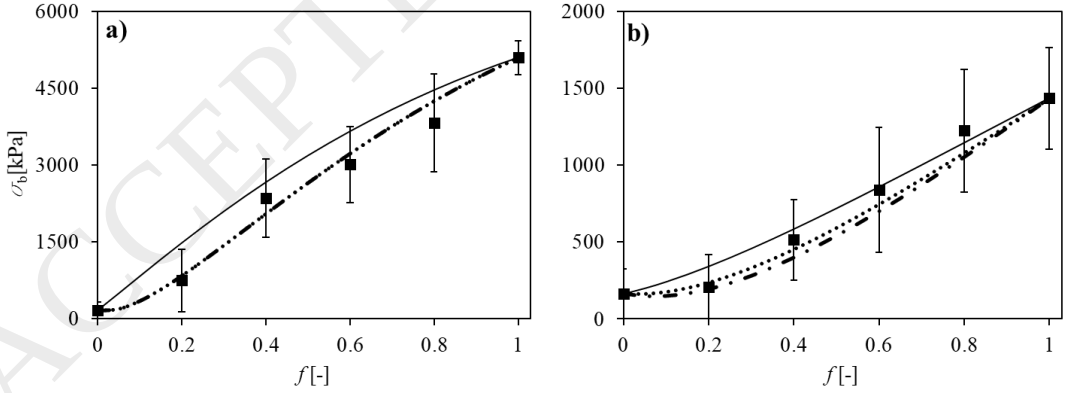

Figure 8. Tensile strength of Ceramic material artefacts as a function of the fines contents for different powder mixtures used in the sintering process: a) MixE, 22.5 µm – 104.2 µm; b) MixF, 51 µm – 104.2 µm; c). Squares are experiments; error bars are standard deviations; lines are model results calculated with different values of the connection force between fine and coarse particles: ––, $F_{fc} = F_{cc}$; .- -, $F_{fc} = 0$; ⋯, F_{fc} minimizes the error with the experiments (values in Table 2). Data point and error bars are the results of 5 independent experiments.

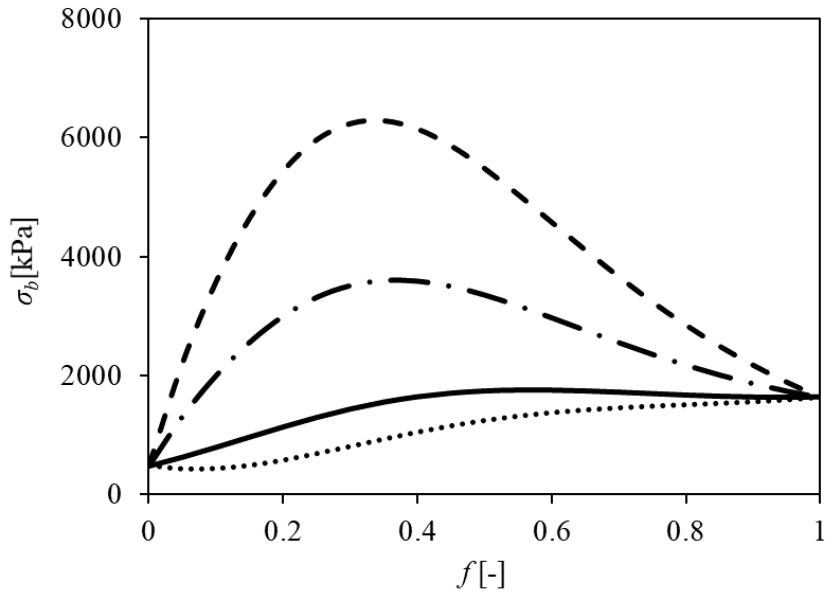

Figure 9. Model results of the sintered material strength as a function of the fines fraction calculated with different values of the connection force between fine and coarse particles: ····, F_{fc}=0; ––, F_{fc}= F_{cc}/2, – · –F_{fc}= F_{cc} and – –, F_{fc}= F_{ff}.

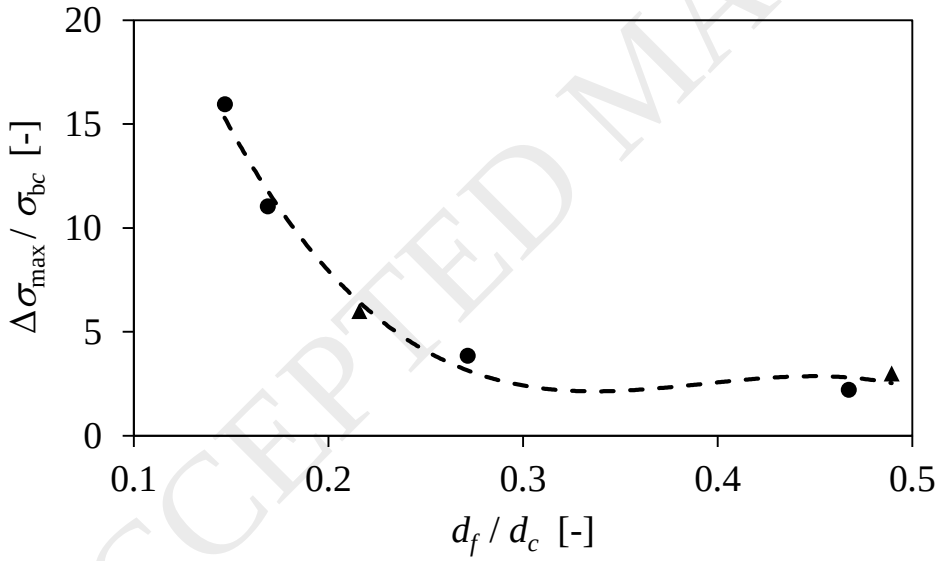

Figure 10. The maximum value of the difference ($\Delta\sigma_{max}$) between the model results for the artefact strength obtained with F_{fc}= F_{cc} and the experimental data, referred to the tensile strength obtained sintering coarse particles only (σ_{bc}) plotted as a function of the fine to coarse particle size ratio d_f/d_c: •, Glass beads; ▲, Ceramic particles; - -, fitted line to guide the eye.

Table 1. Properties of sieved powder samples.

Material	sieving range, μm	d_i, μm	ρ_b, kg m^{-3}	σ_b, mN mm^{-2}	k_i	F_{ii}, mN
Glass	< 25	16	1370	1040	6.85	0.22
	25-63	27	1400	1580	7.07	0.91
	63-90	48	1450	2230	7.39	4.08
	90-125	86	1500	1970	7.94	9.77
	125-180	160	1520	480	8.04	7.88
	180-250	184	1540	180	8.07	3.89
Ceramic	0-20	7.0	711	270	4.52	0.03
	20-38	22.5	915	5090	5.17	3.90
	38-33	40.6	1006	340	5.53	6.60
	63-88	51.0	1101	1430	5.96	4.17
	88-300	104.2	1180	160	6.36	1.74

Table 2. The coding scheme used for bimodal mixtures. The last line of the table reports the fine to coarse particle connection force F_{fc} found with a regression procedure of the model equation (8) on the experimental data relative to each couple of materials at all fines concentrations.

Fines contents	d_i (μm) couples - Glass				d_i (μm) couples – Ceramic	
	27 + 160	86+184	27+184	48+184	22.5 + 104.2	51+104.2
0	A0	B0	C0	D0	E0	F0
20	A1	B1	C1	D1	E1	F1
40	A2	B2	C2	D2	E2	F2
60	A3	B3	C3	D3	E3	F3
80	A4	B4	C4	D4	E4	F4
100	A5	B5	C5	D5	E5	F5
F_{fc}, mN	7.88 10^{-5}	1.95	0.195	7.78 10^{-3}	8.68 10^{-2}	0.867